

Barbie: Text to Barbie-Style 3D Avatars

Xiaokun Sun, Zhenyu Zhang*, Ying Tai, Hao Tang, Zili Yi, Jian Yang



Fig. 1: Our method generates Barbie-style 3D avatars from textual input. “**Barbie-style**” refers to the following key characteristics: (1) **High-Quality** geometry and realistic appearance, ensuring visually lifelike avatars; (2) **Fine-Grained Decoupling**, separating body, clothing, shoes, and accessories to enable flexible apparel combination and editing; (3) **Expressive Animation**, supporting a wide range of body movements, facial expressions, and hand gestures; (4) **Simulation Compatibility**, enabling modeling of non-watertight garments and seamless integration into existing physical simulation pipelines.

Abstract—To integrate digital humans into everyday life, there is a strong demand for generating high-quality, fine-grained disentangled 3D avatars that support expressive animation and simulation capabilities, ideally from low-cost textual inputs. Although text-driven 3D avatar generation has made significant progress by leveraging 2D generative priors, existing methods still struggle to fulfill all these requirements simultaneously. To address this challenge, we propose **Barbie**, a novel text-driven framework for generating animatable 3D avatars with separable shoes, accessories, and simulation-ready garments, truly capturing the iconic “Barbie doll” aesthetic. The core of our framework lies in an expressive 3D representation combined with appropriate modeling constraints. Unlike previous methods, we innovatively employ G-Shell to uniformly model both watertight components (e.g., bodies, shoes, and accessories) and non-watertight garments compatible with simulation. Furthermore, we introduce a well-designed initialization and a hole regularization loss to ensure clean open surface modeling. These disentangled 3D representations are then optimized by specialized expert diffusion models tailored to each domain, ensuring high-fidelity outputs. To mitigate geometric artifacts and texture conflicts when combining different expert models, we further propose several effective geometric losses and strategies. Extensive experiments demonstrate that **Barbie** outperforms existing methods in both dressed human and outfit generation. Our framework further enables

diverse applications, including apparel combination, editing, expressive animation, and physical simulation. Our project page is: <https://xiaokunsun.github.io/Barbie.github.io>

Index Terms—3D disentangled avatar generation, expressive animation, physical simulation, diffusion model, score distillation

I. INTRODUCTION

Automating the creation of 3D avatars without manual effort remains a critical challenge in computer vision and graphics, with applications ranging from VR/AR and virtual try-ons to gaming and beyond [77]–[79]. To fully unlock the potential of these applications, it is essential that the generated avatars meet several key standards: (1) **High Quality**: Digital avatars should feature exquisite geometry and realistic appearances; (2) **Fine-Grained Decoupling**: Enabling separation of body, clothing, shoes, and accessories within the avatar model for flexible customization and editing; (3) **Expressive Animation**: Supporting animations through body movements, facial expressions, and hand gestures; (4) **Simulation Compatibility**: Ensuring that digital avatars dress in non-watertight garments, integrating seamlessly with existing physical simulation pipelines. In vivid terms, we expect the generated digital human with qualities reminiscent of **Barbie dolls**, thereby enhancing their practical value across application scenarios.

Recently, text-driven 3D avatar generation methods [22], [24], [34], which integrate pretrained text-to-image (T2I) diffusion models [9], [10], have gained significant attention by

*Corresponding Author: Zhenyu Zhang (Email: zhangjesse@foxmail.com).

Xiaokun Sun, Zhenyu Zhang, Ying Tai, Zili Yi, and Jian Yang are affiliated with the School of Intelligence Science and Technology, Nanjing University, Jiangsu 215163, China. Email: xiaokun_sun@smail.nju.edu.cn, zhangjesse@foxmail.com, {yingtai, yi, csjyang}@nju.edu.cn.

Hao Tang is affiliated with the School of Computer Science, Peking University, Beijing 100871, China. Email: bjdx tanghao@gmail.com.

This work was supported by the National Science Fund of China under Grant 62376121.

TABLE I: Comparisons of Existing Text-Driven 3D Avatar Generation Methods

Methods	Representation	High Quality	Fine-Grained Decoupling	Expressive Animation	Simulation Compatibility
[22], [24], [25], [30], [31]	NeRF/Neus	✗	✗	✗	✗
[28], [33], [37]	NeRF/Neus	✗	✗	✗	✗
[26], [32]	3DGS	✗	✗	✗	✗
[64]	3DGS	✗	✗	✓	✗
[38]	3DGS	✗	✗	✗	✗
[69]†	3DGS	✗	✗	✗	✓
[23], [36], [80]	SMPL-X	✗	✗	✓	✗
[35]	SMPL-X	✗	✗	✓	✓
[27], [34]	DMTet	✓	✗	✗	✗
Barbie (Ours)	G-Shell	✓	✓	✓	✓

† Although SimAvatar [69] does not separate the body, clothing, shoes, and accessories, it disentangles the body, clothing, and hair. Therefore, we consider it to have achieved fine-grained decoupling.

eliminating the need for human image/video/3D data collection [44], [45], [71], [74], [75], [99]. However, as summarized in Table I, existing text-to-avatar methods fail to meet the above “Barbie-like” standard. Specifically, approaches [22], [24], [25], [28], [30], [31], [33], [37] leveraging implicit NeRF [47], [48] cannot support physical simulation or accurately model facial expressions and hand movements due to a lack of explicit structures. Moreover, these methods tend to produce overly smooth surfaces. Methods [23], [26], [32], [35], [36], [38], [64], [69], [80] using explicit 3DGS [50] and SMPL-X [42] enhance animation expressiveness and simulation compatibility but struggle to capture delicate geometric details. Approaches [27], [34] based on the hybrid representation DMTet [51], integrating strengths of both implicit and explicit 3D representations (*i.e.*, stable optimization properties and explicit structure), are capable of modeling detailed geometry. However, DMTet cannot generate non-watertight surfaces required for realistic garment simulation. Furthermore, current text-to-disentangled-avatar methods typically adopt a single general diffusion model to guide both body and apparel generation. This general constraint compromises in-domain fidelity and fails to produce diverse outfits (*e.g.*, shoes, necklaces, glasses, or other accessories).

It is natural to ask: *Can we automatically generate Barbie-like 3D avatars based on text?* Our answer is yes, but this is a non-trivial task due to several challenges. (1) How do we model watertight components (*e.g.*, bodies, shoes, and accessories) and simulation-ready garments that are non-watertight? While more expressive representations (*e.g.*, G-Shell [63]) offer potential solutions, initializing and regularizing them to accurately represent open surfaces without multi-view image inputs remains an open problem. (2) Providing suitable constraints for optimizing decoupled bodies and outfits to achieve domain-specific realism is both key and challenging.

To address these challenges, we introduce **Barbie**, a novel text-driven framework for generating Barbie-style 3D avatars. As shown in Fig. 1, avatars generated by Barbie not only exhibit exquisite geometry and textures but also feature a variety of decoupled shoes, accessories, and simulation-ready garments that can be freely combined and edited. Furthermore, our framework supports strong animation expressiveness and compatibility with physical simulations, thereby satisfying all four aforementioned requirements simultaneously.

The core of the framework consists of two key components: (1) Unlike previous methods, we employ expressive G-Shell [63] to uniformly model both watertight components

(*e.g.*, bodies, and accessories) and non-watertight garments. Additionally, we design an efficient initialization strategy and a hole-preserving loss to achieve clean and well-defined open surface modeling. (2) Instead of relying on a single general model as in prior text-to-disentangled-avatar methods, we appropriately incorporate different expert diffusion models to guarantee the domain-specific fidelity. A series of effective regularization losses and strategies is also proposed to address geometric artifacts and texture conflicts when combining different expert models. Specifically, our method generates Barbie-like 3D digital humans in three stages: First, we generate a reasonable and realistic base body using human-specific diffusion models along with a proposed SMPLX-evolving prior loss. Second, we initialize apparel with the semantic-aligned body and optimize it using object-specific generative priors and several solid geometric losses. Finally, we jointly fine-tune the assembled avatar to enhance texture harmony and consistency. Through this pipeline, the generated 3D avatars are animatable and disentangled, featuring high-quality bodies, shoes, accessories, and simulation-ready garments, delivering a truly immersive “**Barbie-style**” digital experience.

Our main contributions are summarized as follows:

- We introduce Barbie, a novel text-driven framework for generating realistic and highly disentangled 3D avatars. The framework enables the decoupling of bodies, garments, shoes, and accessories, while enabling outfit transfer, editing, expressive animation, and simulation.
- We innovatively adopt G-Shell to uniformly model watertight and non-watertight components with high fidelity. We further propose an efficient initialization strategy and a hole-preserving loss to ensure clean open surface modeling. To the best of our knowledge, this is the first work to incorporate G-Shell into text-to-3D generation.
- We effectively integrate expert models at different optimization stages to provide suitable guidance, significantly improving the in-domain realism of generated components. Additionally, we introduce a series of geometric losses and strategies to address geometric artifacts and texture conflicts when combining different expert models.
- Extensive experiments demonstrate that Barbie outperforms existing methods in avatar and outfit generation, achieving superior results in geometry quality, texture detail, and alignment with text descriptions.

II. RELATED WORK

Text to Holistic 3D Avatar Generation. The field of text-to-3D generation has witnessed significant progress [12], [14]–[16], [18]–[21], largely driven by advances in text-to-image models [9], [10], [62]. Building upon the success in generating general 3D objects, various methods [22]–[27], [30]–[32], [34], [36], [64], [80] have been proposed to generate complex 3D avatars. AvatarCLIP [22] pioneers zero-shot generation of 3D digital humans from text prompts by leveraging human priors and CLIP [2]. With the introduction of the Score Distillation Sampling (SDS) loss [12], several subsequent works [24], [25], [30], [31] combine it with parametric human models [41], [42], [61] to significantly improve the fidelity of

generated avatars. To enhance animation expressiveness and simulation compatibility, approaches [23], [26], [32], [36], [64], [80] replace implicit NeRF [47], [48] with explicit representations such as 3DGS [50] and SMPL-X [42] for modeling 3D humans. However, purely implicit or explicit representations struggle to capture complex geometric details, limiting the quality of generated digital humans. Accordingly, HumanNorm [34] and SeeAvatar [27] propose using the hybrid representation DMTet [51], which combines the advantages of both implicit and explicit representations to achieve high-fidelity avatar generation. Nevertheless, these methods typically model the human body, garments, shoes, and accessories as a single model, sacrificing flexibility and controllability for downstream applications such as apparel composition and physical simulation.

Text to Disentangled 3D Avatar Generation. To enable controllable avatar creation, several disentangled approaches have been proposed that separately model the human body and outfits through multi-stage optimization. Humancoser [33] and AvatarFusion [28] use two implicit NeRF [47], [48] to represent the body and clothing, respectively. LAGA [38] and TELA [37] adopt a layer-wise framework, modeling each clothing item as an independent layer, further improving generation flexibility and controllability. SO-SMPL [35] and SimAvatar [69] leverage sequentially offset SMPL-X [42] and compositional 3DGS [50] anchored on the mesh to enhance compatibility with simulation pipelines. However, these methods rely on a single general T2I model to guide both body and clothing generation, leading to compromised fidelity in geometry or texture within specific domains. Moreover, they struggle to generate diverse accessories such as shoes, necklaces, glasses, or other fine-grained items.

In contrast, the avatars generated by Barbie not only exhibit exquisite geometry and realistic appearance but also wear multiple separable, realistic outfits, while supporting expressive animation and physical simulation. We summarize the main differences between Barbie and existing methods in Table I.

3D Representation of Decoupled Avatar Modeling. The disentangled modeling of the human body and clothing has been extensively studied in computer vision and graphics. Depending on specific problem settings, different representations are chosen based on trade-offs among optimization properties, geometric modeling capabilities, animation expressiveness, and simulation compatibility: **(1) Implicit representations** [47], [48], [68], [85] are widely adopted in decoupled 3D avatar reconstruction and generation tasks [28], [33], [37], [67] due to their stable optimization properties. However, they lack explicit structures, making them unsuitable for expressive animation and physical simulation. **(2) Explicit representations** [41], [42], [50] are commonly used in disentangled digital human creation [35], [38], [69], [81], [84], as they provide explicit structures suitable for animation and simulation. Nevertheless, they struggle to capture delicate geometric details. **(3) Combinations of the above representations** have also been proposed to achieve high-fidelity reconstruction and generation of decoupled 3D avatars [86]–[89]. Despite these efforts, the inherent disadvantages mentioned above persist. **(4) Hybrid representations** [51], [63] combine the

advantages of implicit and explicit representations to sculpt impressive geometric details in reconstructed disentangled 3D avatars [65], [83]. G-Shell [63], in particular, addresses the limitation that DMTet [51] cannot model non-watertight surfaces compatible with physical simulations. However, how to initialize and regularize G-Shell without strong multi-view image input remains an open problem. In this work, we aim to unlock the potential of G-Shell for the challenging task of text-driven Barbie-style 3D avatar generation.

III. METHOD

A. Preliminary

SMPL-X [42] is a parametric human model that represents the shape, pose, and expression using a set of parameters. Given shape parameters β , body pose parameters θ_{body} , jaw pose parameters θ_{jaw} , hand pose parameters θ_{hand} , and expression parameters ψ_{exp} , it generates a 3D human mesh M_{smplx} .

Score Distillation Sampling [12] leverages a pre-trained T2I model to guide the alignment of a 3D representation with input text. Given a text prompt y , a 3D representation parameterized by θ , and a diffusion model parameterized by ϕ , the SDS loss is defined as:

$$\nabla_{\theta} \mathcal{L}_{SDS} = \mathbb{E}_{t, \epsilon} \left[w(t) (\epsilon_{\phi}(x_t; y, t) - \epsilon) \frac{\partial x}{\partial \theta} \right], \quad (1)$$

where t is the time step in the 2D diffusion process, $x = g(\theta)$ is the image rendered from θ by a differentiable renderer [52] $g(\cdot)$, $x_t = x + \epsilon$ is a noised version of x , $\epsilon_{\phi}(x_t; y, t)$ is the denoised image, and $w(t)$ is the weight function. For simplicity, we omit $w(t)$ in the following formulas.

DMTet [51] is a hybrid representation that combines an implicit signed distance field (SDF) $s : \mathbb{R}^3 \mapsto \mathbb{R}$ and a differentiable Marching Tetrahedral layer $DMT(\cdot)$ to transfer an implicit SDF into an explicit watertight mesh M_{wt} . This process is formulated as: $M_{wt} = DMT(s(q))$, where q is a set of predefined sampled points. By integrating the strengths of both implicit and explicit 3D representations (*i.e.*, stable optimization properties and explicit structure), DMTet enables high-fidelity geometric modeling.

G-Shell [63] is an expressive representation capable of modeling both watertight and non-watertight surfaces. Building upon DMTet, G-Shell introduces a manifold signed distance field (mSDF) $\hat{s} : \mathbb{R}^3 \mapsto \mathbb{R}$ on a watertight template. In this field, the sign indicates whether a point lies on an open surface, while the absolute value represents the geodesic distance to the boundary. A non-watertight mesh M_{nwt} can then be extracted through the G-Shell mesh extraction process $GSE(\cdot)$: $M_{nwt} = GSE(s(q), \hat{s}(q))$. Additionally, G-Shell can also model a watertight mesh M_{wt} by ignoring mSDF. In this case, G-Shell is equivalent to DMTet: $M_{wt} = GSE(s(q))$.

B. Overview

Given a text prompt, Barbie aims to create an animatable, disentangled 3D avatar dressed in simulation-ready garments, along with diverse shoes and accessories, resembling iconic Barbie dolls. Specifically, our framework consists of three stages: **(1) Human Body Generation:** This stage generates

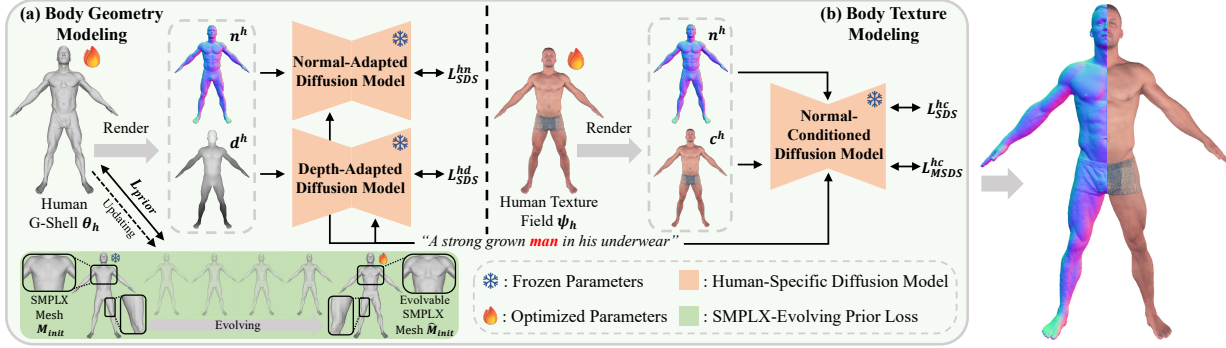


Fig. 2: The process for generating a basic human model involves two steps: **(a)** Employing human-specific geometry-aware diffusion models and the SMPLX-evolving prior loss to model realistic and reasonable body shapes. **(b)** Subsequently, using a normal-conditioned diffusion model to generate lifelike human textures.

a reasonable and realistic basic human body by leveraging human-specific generative priors and a novel SMPLX-evolving prior loss (Sec. III-C and Fig. 2); **(2) Apparel Generation:** This stage models high-quality garments, shoes, and accessories piece by piece, utilizing object-specific diffusion models together with several initialization strategies and geometric losses (Sec. III-D and Fig. 3); and **(3) Unified Texture Refinement:** This stage enhances visual harmony and consistency by jointly fine-tuning the composed avatar (Sec. III-E and Fig. 3).

C. Human Body Generation

Since the human body is a closed surface, we utilize G-Shell θ_h in watertight mesh mode (*i.e.*, ignoring mSDF and retaining only SDF) and a texture field ψ_h to model the geometry and appearance of the human body, respectively. These components are optimized under human-specific generative priors and a novel SMPLX-evolving prior loss, as illustrated in 2.

Human Body Geometry Modeling. To enhance the robustness of 3D human generation, we start by initializing the human G-Shell θ_h with an SMPL-X model M_{init} . This SMPL-X mesh M_{init} will be used in subsequent stages to provide rich human priors and ensure a semantic-aligned representation for outfit creation. As discussed in the introduction, using a general T2I model struggles to provide domain-specific constraints necessary for creating realistic human bodies or outfits. To address this limitation, we employ human-specific diffusion models from HumanNorm [34], which is fine-tuned with high-fidelity human data.

In particular, the human-specific diffusion models include a normal-adapted diffusion model ϕ_{hn} , a depth-adapted diffusion model ϕ_{hd} for human shape generation, and a normal-conditioned diffusion model ϕ_{hc} for human texture creation. The geometry-aware diffusion models optimize the initialized human G-Shell θ_h using the following SDS losses:

$$\nabla_{\theta_h} \mathcal{L}_{SDS}^{hn} = \mathbb{E}_{t,\epsilon} \left[(\epsilon_{\phi_{hn}}(n_t^h; y_h, t) - \epsilon) \frac{\partial n^h}{\partial \theta_h} \right], \quad (2)$$

$$\nabla_{\theta_h} \mathcal{L}_{SDS}^{hd} = \mathbb{E}_{t,\epsilon} \left[(\epsilon_{\phi_{hd}}(d_t^h; y_h, t) - \epsilon) \frac{\partial d^h}{\partial \theta_h} \right], \quad (3)$$

where n^h and d^h are the rendered normal and depth maps of the human body, respectively. y_h denotes the input minimal-clothed human body description.

SMPLX-Evolving Prior Loss. Although Eq. 2 and Eq. 3 enable the creation of intricate human bodies, the overly strong human-specific generative priors cause the generated results to overfit the input text. This leads to unnatural geometry and exaggerated body proportions (Fig. 8-(a)). A straightforward approach is to introduce parametric human body models (*e.g.*, SMPL-X) and provide human body priors using the following equation:

$$\mathcal{L}_{prior} = \sum_{p \in P} \|s_{\theta_h}(p) - s_{init}(p)\|_2^2, \quad (4)$$

where $s_{\theta_h}(\cdot)$ and $s_{init}(\cdot)$ represent the SDF of the generated body G-Shell θ_h and the initialized SMPL-X mesh M_{init} , respectively, and P is a set of randomly sampled points in space. However, due to the overly smooth geometry of SMPL-X, this approach may lead to a reduction in diversity and fine details (Fig. 8-(a)).

To address this problem, we propose the SMPLX-evolving prior loss inspired by the evolving constraint introduced in SeeAvatar [27]. Specifically, we freeze the SMPL-X shape parameters β but enhance M_{init} to an evolvable \hat{M}_{init} by adding learnable vertex-wise offsets. These offsets are periodically fitted to the current body every δ iteration, allowing the optimized offsets to model complex body features. The fitting objective is as follows:

$$\mathcal{L}_{fit} = \lambda_{chamf} \mathcal{L}_{chamf} + \lambda_{edge} \mathcal{L}_{edge} + \lambda_{nor} \mathcal{L}_{nor} + \lambda_{lap} \mathcal{L}_{lap}, \quad (5)$$

where \mathcal{L}_{chamf} is the Chamfer distance between \hat{M}_{init} and the current body shape, \mathcal{L}_{edge} , \mathcal{L}_{nor} and \mathcal{L}_{lap} are the edge length regularization, normal consistency loss, and Laplacian smoothness, respectively. The advantages of this loss are twofold: **(1) Enhanced Modeling Capabilities:** Compared to the smooth M_{init} , our \hat{M}_{init} excels at capturing detailed geometric features, such as muscle contours (see the zoomed area at the bottom of Fig. 2), and offers reliable yet diverse priors for subsequent geometry generation (Fig. 8-(a)). **(2) Topology Preservation:** Unlike the evolving templates with arbitrary topology in SeeAvatar [27], our \hat{M}_{init} preserves the SMPL-X model's topology and semantics during the evolution process. This makes it particularly suitable for apparel initialization, composition, animation, and simulation (Fig. 9).

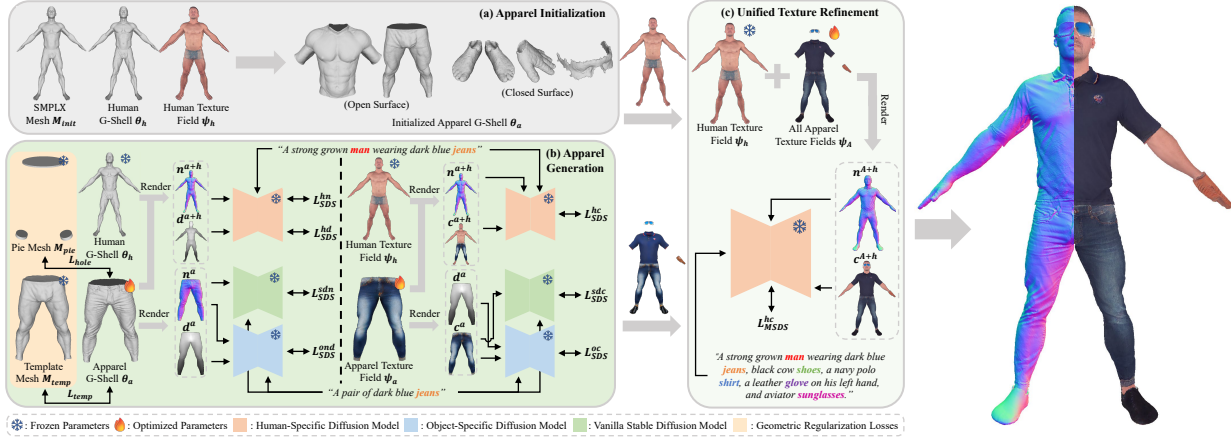


Fig. 3: The process for generating apparel involves three steps: (a) Initializing apparel with the semantic-aligned human body. (b) Modeling apparel piece by piece using object-specific generative priors and geometric losses. (c) Refining the texture of the assembled avatar using a unified texture refinement process.

In summary, the loss function for optimizing the human body geometry is formulated as follows:

$$\mathcal{L}_{hum-geo} = \mathcal{L}_{SDS}^{hn} + \mathcal{L}_{SDS}^{hd} + \lambda_{prior} \mathcal{L}_{prior}. \quad (6)$$

Human Body Texture Modeling. Given the human mesh generated from the previous stage, we fix it and utilize a texture field ψ_h which maps a query position to its color to generate a normal-aligned body appearance. This field is optimized using a normal-conditioned diffusion model ϕ_{hc} with loss defined as:

$$\nabla_{\psi_h} \mathcal{L}_{SDS}^{hc} = \mathbb{E}_{t,\epsilon} \left[\left(\epsilon_{\phi_{hc}}(c_t^h; n^h, y_h, t) - \epsilon \right) \frac{\partial c^h}{\partial \psi_h} \right], \quad (7)$$

where c^h represents the rendered color image of the generated human body. Since the vanilla SDS loss often leads to color oversaturation, we replace it with the following multi-step SDS (MSDS) loss [34] to further enhance the texture's realism in later iterations of texture optimization:

$$\begin{aligned} \nabla_{\psi_h} \mathcal{L}_{MSDS}^{hc} = & \mathbb{E}_{t,\epsilon} \left[\left(h(c_t^h; n^h, y_h, t) - \epsilon \right) \frac{\partial c^h}{\partial \psi_h} \right] + \\ & \mathbb{E}_{t,\epsilon} \left[\left(V(h(c_t^h; n^h, y_h, t)) - V(\epsilon) \right) \frac{\partial V(\epsilon)}{\partial \epsilon} \frac{\partial c^h}{\partial \psi_h} \right], \end{aligned} \quad (8)$$

where V denotes the first k layers of the VGG network [90], and $h(\cdot)$ represents the multi-step image generation function of the normal-aligned diffusion model.

D. Apparel Generation

Given an SMPLX-aligned basic body generated in the previous stage, we proceed to dress the Barbie avatar in various outfits. Similar to body modeling, we employ G-Shell θ_a for apparel geometry and a texture field ψ_a for apparel texture. Closed shoes and accessories are represented using G-Shell in watertight mesh mode (*i.e.*, ignoring mSDF and retaining only SDF), while open garments are modeled using G-Shell in non-watertight mesh mode (*i.e.*, retaining both SDF and mSDF). As illustrated in Fig. 3, the apparel generation process begins by initializing apparel using predefined SMPL-X masks that cover

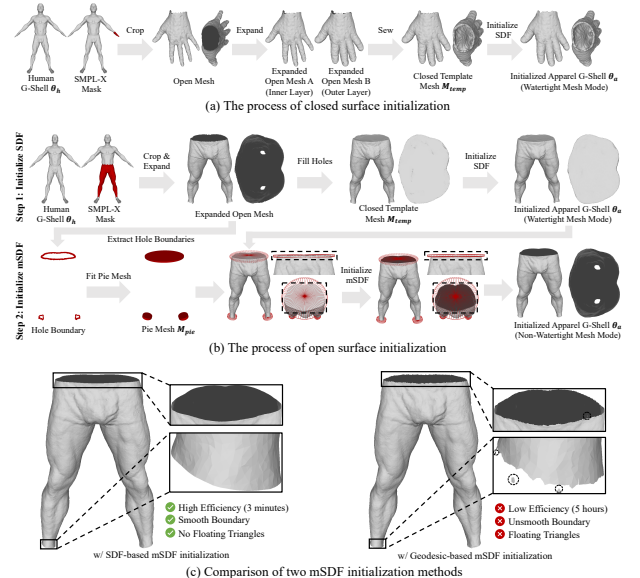


Fig. 4: (a) **Closed Surface Initialization:** Expand and sew the open mesh (cropped via SMPL-X mask) to create a closed template mesh M_{temp} , used to initialize the SDF $s_{\theta_a}(\cdot)$ of θ_a . (b) **Open Surface Initialization:** Fit a watertight pie mesh M_{pie} over the holes of the cropped open mesh. Use its SDF values to initialize the mSDF $\hat{s}_{\theta_a}(\cdot)$ of θ_a . (c) **Comparison:** Contrast geodesic-based and SDF-based mSDF initialization.

over a dozen daily outfits. We then create high-quality apparel piece by piece using object-specific generative priors and well-designed geometric losses. Lastly, we fine-tune the assembled avatar to improve appearance harmony and consistency.

Apparel Initialization. Due to the lack of reliable multi-view image input [63], [65], initialization plays a critical role in text-driven G-Shell optimization. Therefore, we carefully design two strategies for initializing open clothes and closed shoes/accessories, enabling accurate topology modeling for each category. **(1) Closed Surface Initialization:** We crop the open sub-mesh of the human body using the corresponding SMPL-X mask, expand it along vertex normals to create inner

and outer layers, and sew them to form a double-layer closed template mesh M_{temp} . This mesh initializes the SDF $s_{\theta_a}(\cdot)$ of the apparel G-Shell θ_a . Fig. 4-(a) shows this process. **(2) Open Surface Initialization:** Since mSDF is defined on a watertight surface, we first initialize the SDF $s_{\theta_a}(\cdot)$ of θ_a . Concretely, we expand the cropped open mesh, fill its holes, and obtain a single-layer watertight template mesh M_{temp} . Unlike the double-layer template mesh in closed surface initialization, this simpler template mesh is better suited for mSDF initialization. The initialization of mSDF is the core of the open surface initialization process. A straightforward way is to initialize mSDF according to its definition (*i.e.*, the signed geodesic distance to the open surface boundary on the watertight template). Nonetheless, this geodesic-based approach is not only computationally expensive (5 hours) but also unstable, often causing unsound boundaries and floating triangles (Fig. 4-(c)). This is because geodesics are defined on the surface and cannot stably supervise a 3D implicit field.

To solve these issues, we propose a novel SDF-based mSDF initialization strategy. Specifically, we fit a pie-shaped watertight mesh M_{pie} to each hole that covers its boundaries (see the Supp. Mat. for fitting details). We then use M_{pie} 's SDF values to initialize the mSDF $\hat{s}_{\theta_a}(\cdot)$ of θ_a . In this way, we can remove intersections between M_{temp} and M_{pie} , thereby obtaining the desired open surface (see the black dotted box in Fig. 4-(b)). Fig. 4-(b) illustrates the whole process. Our method offers three key advantages: **(1) Efficiency:** Computing SDF takes only about 3 minutes, significantly faster than computing geodesics (5 hours). **(2) Stability:** The SDF defined in 3D space can stably supervise the 3D implicit field, thus effectively avoiding floating triangles and unsound boundaries. **(3) Feature Mesh:** M_{pie} provides regularization constraints for subsequent optimization (see Eq. 14). Fig. 4-(c) compares the two initialization methods.

Apparel Geometry Modeling. Similar to human body geometry generation, we utilize human-specific diffusion models to optimize outfit geometry with the SDS loss:

$$\nabla_{\theta_a} \mathcal{L}_{SDS}^{hn} = \mathbb{E}_{t,\epsilon} \left[(\epsilon_{\phi_{hn}}(n_t^{a+h}; y_{a+h}, t) - \epsilon) \frac{\partial n^{a+h}}{\partial \theta_a} \right], \quad (9)$$

$$\nabla_{\theta_a} \mathcal{L}_{SDS}^{hd} = \mathbb{E}_{t,\epsilon} \left[(\epsilon_{\phi_{hd}}(d_t^{a+h}; y_{a+h}, t) - \epsilon) \frac{\partial d^{a+h}}{\partial \theta_a} \right], \quad (10)$$

where y_{a+h} is the text description of the clothed avatar, and n^{a+h} and d^{a+h} are the rendered clothed human normal and depth maps, respectively. However, human-specific diffusion models are not well-suited for creating high-quality clothes, shoes, and accessories because they are not good at modeling general 3D objects. Hence, we additionally introduce the object-specific diffusion models [18] pretrained on the LAION dataset [46] for providing in-domain details and diversity.

Concretely, these diffusion models include a normal-depth diffusion model ϕ_{ond} for optimizing the apparel geometry, and a depth-conditional diffusion model ϕ_{oc} for creating the apparel texture. The normal-depth model provides effective supervision for outfit geometry generation by accurately modeling the joint distribution of normal and depth maps using

the following SDS loss:

$$\begin{aligned} \nabla_{\theta_a} \mathcal{L}_{SDS}^{ond} &= \mathbb{E}_{t,\epsilon} \left[(\epsilon_{\phi_{ond}}(n_t^a; y_a, t) - \epsilon) \frac{\partial n^a}{\partial \theta_a} \right] \\ &+ \mathbb{E}_{t,\epsilon} \left[(\epsilon_{\phi_{ond}}(d_t^a; y_a, t) - \epsilon) \frac{\partial d^a}{\partial \theta_a} \right], \end{aligned} \quad (11)$$

$$\nabla_{\theta_a} \mathcal{L}_{SDS}^{sdn} = \mathbb{E}_{t,\epsilon} \left[(\epsilon_{\phi_{sd}}(n_t^a; y_a, t) - \epsilon) \frac{\partial n^a}{\partial \theta_a} \right], \quad (12)$$

where y_a is the description of a single outfit, and n^a and d^a are the rendered normal and depth maps of the apparel in the undressed state. Besides, \mathcal{L}_{SDS}^{sdn} is the vanilla Stable Diffusion (SD) SDS loss enforced on the rendered apparel normal maps. As shown in RichDreamer [18], naive SD helps object-specific diffusion models produce more stable results. In this way, the object-specific diffusion models provide powerful guidance to modeling high-fidelity outfits (Fig. 8-(b)).

Template-Preserving Loss. Similar to human-specific diffusion models, relying on object-specific diffusion models may lead to geometric artifacts (*e.g.*, unexpected holes, see Fig. 8-(d)). To address this problem, we propose a template-preserving loss that enforces the apparel geometry to fit the template mesh M_{temp} , ensuring geometric integrity. This loss is formulated as follows:

$$\mathcal{L}_{temp} = \sum_{p \in P} \|s_{\theta_a}(p) - s_{temp}(p)\|_2^2, \quad (13)$$

where $s_{temp}(\cdot)$ represents the SDF of the template mesh M_{temp} , and P is the set of randomly sampled points in space.

Hole-Preserving Loss. Since the object-specific diffusion model is primarily trained on watertight mesh data, it tends to guide the G-Shell to model closed surfaces, resulting in many floating triangles inside the holes (Fig. 8-(e)). Moreover, due to the absence of multi-image input, we cannot reliably supervise the open surface like other G-Shell reconstruction works [63], [65]. To address this issue, we propose a hole-preserving loss that exploits the pie mesh M_{pie} obtained from the SDF-based mSDF initialization. This loss is formulated as:

$$\mathcal{L}_{hole} = \sum_{p \in P} \|\hat{s}_{\theta_a}(p) - s_{pie}(p)\|_2^2, \quad (14)$$

where $s_{pie}(\cdot)$ represents the SDF of the pie mesh M_{pie} . This loss effectively suppresses floating triangles by using the SDF of M_{pie} to supervise the mSDF of θ_a , thereby preserving clean and well-defined hole structures.

Collision Loss. To ensure the generated apparel does not intersect with the underlying human body (Fig. 8-(f)), we introduce the following collision loss \mathcal{L}_{colli} :

$$\mathcal{L}_{colli} = \sum_{v \in V} \text{relu}(-s_h(v)), \quad (15)$$

where V is the set of vertices of the generated apparel mesh, and $s_h(\cdot)$ is the SDF of the human body.

In summary, the loss function for optimizing the apparel geometry is as follows:

$$\begin{aligned} \mathcal{L}_{app-geo} &= \mathcal{L}_{SDS}^{hn} + \mathcal{L}_{SDS}^{hd} + \mathcal{L}_{SDS}^{ond} + \mathcal{L}_{SDS}^{sdn} \\ &+ \lambda_{temp} \mathcal{L}_{temp} + \lambda_{hole} \mathcal{L}_{hole} + \lambda_{colli} \mathcal{L}_{colli}, \end{aligned} \quad (16)$$



Fig. 5: Diverse Range of **Barbie-Style** Avatar Generation. Rendering color images and normal images for visualization. **Please zoom in to see the details and see Supp. Mat. for video results.**

where \mathcal{L}_{hole} is only used in non-watertight mesh mode.

Apparel Texture Modeling. Given the generated apparel shape and the textured human body, we employ an object-specific depth-conditional diffusion model for lifelike apparel textures with the following SDS loss:

$$\nabla_{\psi_a} \mathcal{L}_{SDS}^{oc} = \mathbb{E}_{t,\epsilon} \left[(\epsilon_{\phi_{oc}}(c_t^a; d^a, y_a, t) - \epsilon) \frac{\partial c^a}{\partial \psi_a} \right], \quad (17)$$

$$\nabla_{\psi_a} \mathcal{L}_{SDS}^{sdc} = \mathbb{E}_{t,\epsilon} \left[(\epsilon_{\phi_{sd}}(c_t^a; y_a, t) - \epsilon) \frac{\partial c^a}{\partial \psi_a} \right], \quad (18)$$

where c^a is the color image. Additionally, human-specific diffusion models are combined to optimize the appearance of outfits in the dressed state to ensure basic texture harmony, and the SDS loss is formulated as:

$$\nabla_{\psi_a} \mathcal{L}_{SDS}^{hc} = \mathbb{E}_{t,\epsilon} \left[(\epsilon_{\phi_{hc}}(c_t^{a+h}; n^{a+h}, y_{a+h}, t) - \epsilon) \frac{\partial c^{a+h}}{\partial \psi_a} \right]. \quad (19)$$

In summary, the loss function for optimizing the apparel appearance is as follows:

$$\mathcal{L}_{app-tex} = \mathcal{L}_{SDS}^{hc} + \mathcal{L}_{SDS}^{oc} + \mathcal{L}_{SDS}^{sdc}. \quad (20)$$

E. Unified Texture Refinement

After the above steps, we produce detailed geometry and lifelike textures for human bodies, garments, shoes, and accessories. However, a domain gap in the training data for fine-tuning expert models causes texture disharmony between the body and outfits, reducing realism (Fig. 8-(c)). To address this issue, we propose a unified texture refinement (UTR) strategy. Specifically, we fine-tune all apparel texture fields $\psi_A = \{\psi_{a_i}, i \in [1, \dots, N]\}$ of the assembled avatar under the human-specific normal-conditioned diffusion model and the MSDS loss from Eq.8. The UTR strategy ensures visual unity and improves texture harmony across the avatar. It reduces the domain gap, enhancing realism and aesthetic quality.

F. Implementation Details

Our algorithm is implemented using PyTorch [56] and Three-Studio [57]. We use MLP with multi-resolution hash encoding [49] to efficiently represent SDF, mSDF, and color fields. Given a text describing a dressed human, e.g., “A man wearing X1 and X2”, we first generate a base human body based on “A man in his underwear”. We then generate the apparel X1 based on “A piece of X1” and “A man wearing X1”, and then generate the apparel X2 based on “A piece of X2” and

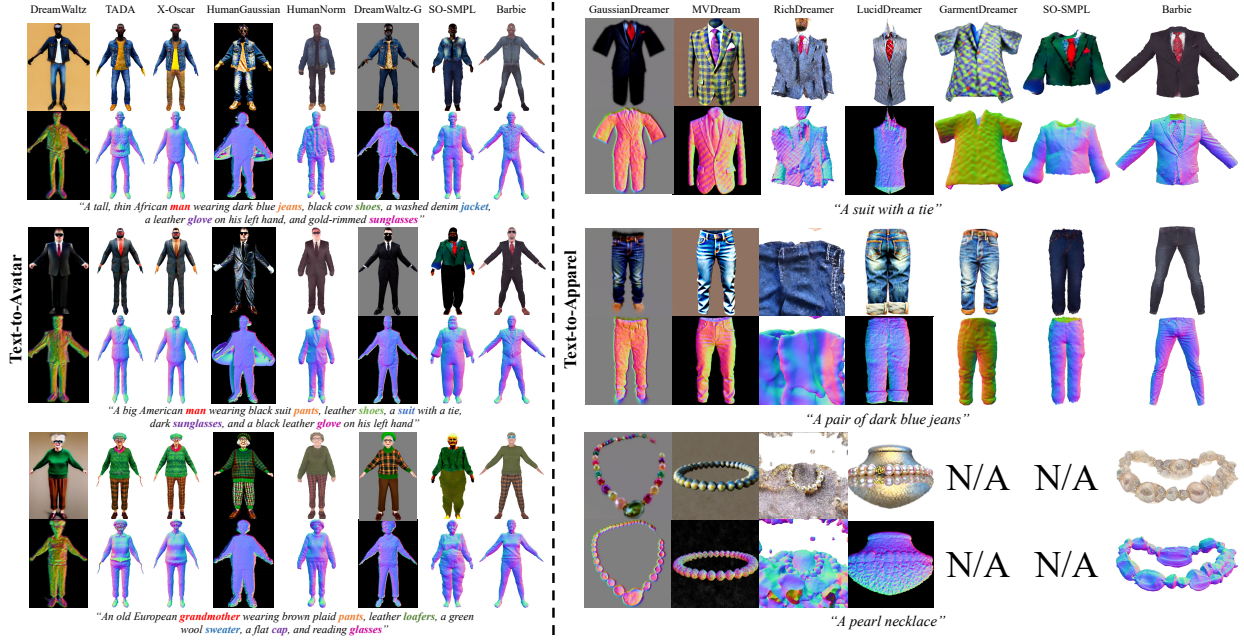


Fig. 6: Qualitative comparisons with baseline text-to-avatar and text-to-apparel methods. GarmentDreamer [39] and SO-SMPL [35] only support clothing generation.

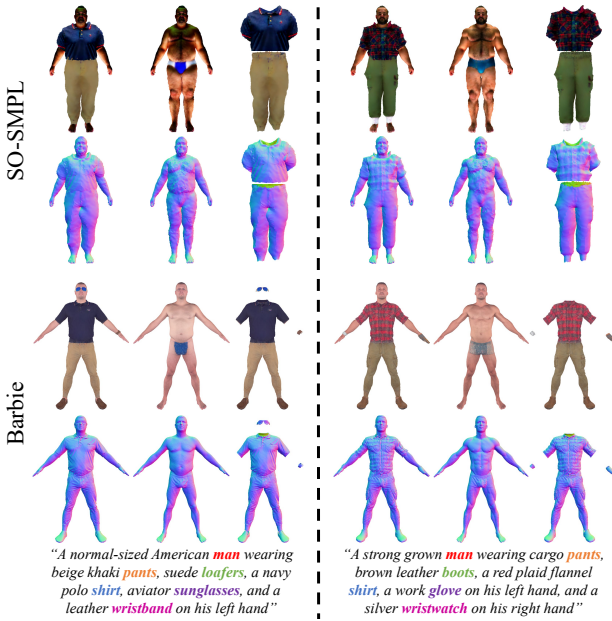


Fig. 7: Qualitative comparisons with the text-to-disentangled-avatar work SO-SMPL [35]. SO-SMPL not only exhibits significantly lower generation quality than our method but also fails to produce the diverse outfits shown in Fig. 5, as achieved by our Barbie-style avatars.

“A man wearing X1 and X2”. Finally, fine-tune the overall texture based on the full input text “A man wearing X1 and X2”. Additional details can be found in Supp. Mat.

IV. EXPERIMENTS

Some examples of 3D bodies and outfits generated by our method are shown in Fig. 5. Due to space limitations, only

TABLE II: Quantitative comparisons with baseline methods

Method	BLIP-VQA \uparrow	BLIP2-VQA \uparrow	GQP \uparrow	TAP \uparrow
DreamWaltz	0.5819	0.5333	3.67	3.67
TADA	0.5306	0.5333	4.67	5.00
X-Oscar	0.5069	0.5292	4.00	4.00
HumanGaussian	0.6222	0.5069	3.67	3.00
HumanNorm	0.5611	0.5292	5.00	3.33
DreamWaltz-G	0.6444	0.5722	2.33	3.33
SO-SMPL	0.6500 [†]	0.6000 [†]	0.00	0.67
Barbie (Ours)	0.7167/0.7333[†]	0.6333/0.7000[†]	76.67	77.00
MVDream	0.7000	0.5933	12.33	12.00
GaussianDreamer	0.7017	0.5283	5.00	5.33
RichDreamer	0.8100	0.6667	2.67	5.00
LucidDreamer	0.7533	0.6400	6.67	5.33
GarmentDreamer	0.6500 [†]	0.4500 [†]	1.00	1.00
SO-SMPL	0.8500 [†]	0.7667 [†]	0.00	0.00
Barbie (Ours)	0.8667/0.9667[†]	0.7667/0.9167[†]	72.33	71.33

The best result is highlighted in **bolded**. GQP: generation quality preference (%), TAP: text-image alignment preference (%). [†]: When calculating VQA metrics, we ignore the problem of retrieving shoes and accessories, as GarmentDreamer [39] and SO-SMPL [35] not only support clothing generation.

the key experimental settings and results are presented here. For complete results and details, please refer to our Supp. Mat.

A. Experimental Settings

Baselines. We perform both quantitative and qualitative comparisons of Barbie with state-of-the-art (SOTA) SDS-based methods for text-driven avatar generation and apparel generation. For avatar generation, we compare with text-to-holistic-avatar methods (DreamWaltz [31], TADA [23], X-Oscar [36], HumanGaussian [32], HumanNorm [34], and DreamWaltz-G [64]) and text-to-decoupled-avatar method (SO-SMPL [35]). For text-to-apparel generation, we compare with text-to-3D methods (MVdream [16], GaussianDreamer [19], RichDreamer [18], LucidDreamer [21]), text-to-garment method (GarmentDreamer [39]), and SO-SMPL [35].

Dataset Construction. We utilized ChatGPT [1] to randomly generate 30 text descriptions of dressed avatars, with each example wearing a top, a bottom, a pair of shoes, and two

random accessories. 30 descriptions for dressed humans are used to evaluate avatar generation, and 30×5 apparel descriptions are used to evaluate apparel generation (see the Supp. Mat. for the complete descriptions).

Evaluation Metrics. Existing text-to-3D approaches utilize CLIP-based metrics to evaluate text-image alignment and compare the quality of generated results. However, CLIP-based metrics have been shown [4], [5] to be insufficient to accurately measure the fine-grained correspondence between 3D content and input prompts, which is further confirmed by experiments in the Supp. Mat.

Consequently, inspired by Progressive3D [55], we adopt fine-grained text-to-image evaluation metrics, including BLIP-VQA [58], [59] and BLIP2-VQA [58], [60], to evaluate the generation capacity of current methods and Barbie. Specifically, we first convert the prompt into multiple separate questions to retrieve corresponding content, then feed the rendered image of the generated content into the VQA model and ask questions one by one, and finally use the probability of answering “yes” as the evaluation metric. For instance, the input avatar prompt “A man wearing X1.” is converted into “Is the person in the picture a man?” and “Is the person in the picture wearing X1?”. The input apparel prompt “A pair of X1.” is converted into “Is the object in the picture a pair of X1?”. Besides, we randomly select 10 examples from the generated results to conduct a user study and ask 30 volunteers to assess (1) generation quality and (2) text-image alignment, and select the preferred methods.

B. Comparisons of Avatar Generation

Comparison with Text-to-Avatar Methods. As shown in the upper part of Table II, our method significantly outperforms all baseline methods across all evaluation metrics. The qualitative results presented in the left part of Fig. 6 further validate its superiority. Compared to existing methods, Barbie generates avatars with more detailed and realistic geometry, while achieving better alignment with the input text, without omitting any specified apparel items. Moreover, Barbie achieves a high degree of disentanglement among body, garments, shoes, and accessories, enabling flexible outfit combinations and edits, much like dressing physical Barbie dolls (Fig. 9-(a) and -(b)). Furthermore, thanks to the use of G-Shell and the proposed SMPLX-evolving prior loss, Barbie supports expressive animation and compatibility with physical simulation (Fig. 9-(c) and -(d)).

Comparison with Text-to-Decoupled-Avatar Method. As illustrated in Fig. 7, our method surpasses SO-SMPL [35] in generating finer geometric details and more lifelike textures. Additionally, Barbie enables the generation of various accessories (e.g., necklaces, glasses, and watches), which are not supported by SO-SMPL [35].

C. Comparisons of Apparel Generation

As shown in the lower part of Table II, our approach consistently outperforms all competing methods on all evaluation metrics. Qualitative comparisons are shown in the right part of Fig. 6, displaying representative generated outfits. Compared

to other methods, Barbie produces apparel with higher-fidelity geometry and textures, while maintaining accurate alignment with the input text, without introducing irrelevant elements such as body parts. Thanks to the expressive G-Shell [63] representation, we are able to accurately model the non-watertight topology of garments, enabling compatibility with physical simulations (Fig. 9-(d)).

D. Ablation Study

We conduct detailed ablation studies in Fig. 8 to validate the effectiveness of each component in Barbie.

Effect of SMPLX-Evolving Prior Loss. As shown in Fig. 8-(a), omitting \mathcal{L}_{prior} leads to distorted body proportions and unnatural hands, significantly degrading realism. Using a fixed human prior ensures anatomical plausibility but results in overly smooth surfaces with limited detail (e.g., missing muscle contours and hair). In contrast, the full \mathcal{L}_{prior} enables both reasonable and detailed human body generation while providing rich semantics that support downstream tasks such as apparel transfer, editing, animation, and simulation.

Effect of Object-Specific Diffusion Models. To enhance in-domain outfit fidelity, we employ object-specific diffusion models for generating apparel geometry and texture. As illustrated in Fig. 8-(b), object-specific generative priors significantly enhance the visual quality of generated outfits, particularly in geometric detail.

Effect of Unified Texture Refinement. To reduce visual inconsistency between the body and outfits, we introduce a unified texture refinement (UTR) strategy. Fig. 8-(c) confirms that UTR effectively reduces texture conflicts across components, thereby enhancing overall realism and aesthetic coherence.

Effect of Template-Preserving Loss. To preserve structural integrity in the generated apparel, we incorporate a template-preserving loss \mathcal{L}_{temp} . As shown in Fig. 8-(d), this loss is essential for preventing unexpected holes and other geometric artifacts that severely degrade apparel quality.

Effect of Hole-Preserving Loss. To accurately model intended garment openings (e.g., necklines), we propose \mathcal{L}_{hole} . As demonstrated in Fig. 8-(e), \mathcal{L}_{hole} avoids floating triangles within holes, resulting in clean neckline structures.

Effect of Collision Loss. To avoid intersections between apparel and the underlying body, we introduce \mathcal{L}_{coll} . As illustrated in Fig. 8-(f), neglecting \mathcal{L}_{coll} causes severe collision artifacts, which notably compromise result realism.

E. Applications

As shown in Fig. 9-(a) and -(b), Barbie’s fine-grained decoupling enables the free combination and editing of any human body and outfit, similar to dressing physical Barbie dolls. This significantly enhances the playability and reusability of text-to-avatar generation. Thanks to the SMPLX-evolving prior loss \mathcal{L}_{prior} , we achieve accurate alignment between the generated assets and the SMPL-X model, enabling natural full-body animation involving facial expressions, body poses, and hand gestures, as demonstrated in Fig. 9-(c). The expression sequences are taken from TalkShow [92], and the body motions from AIST++ [93]. Furthermore, leveraging the

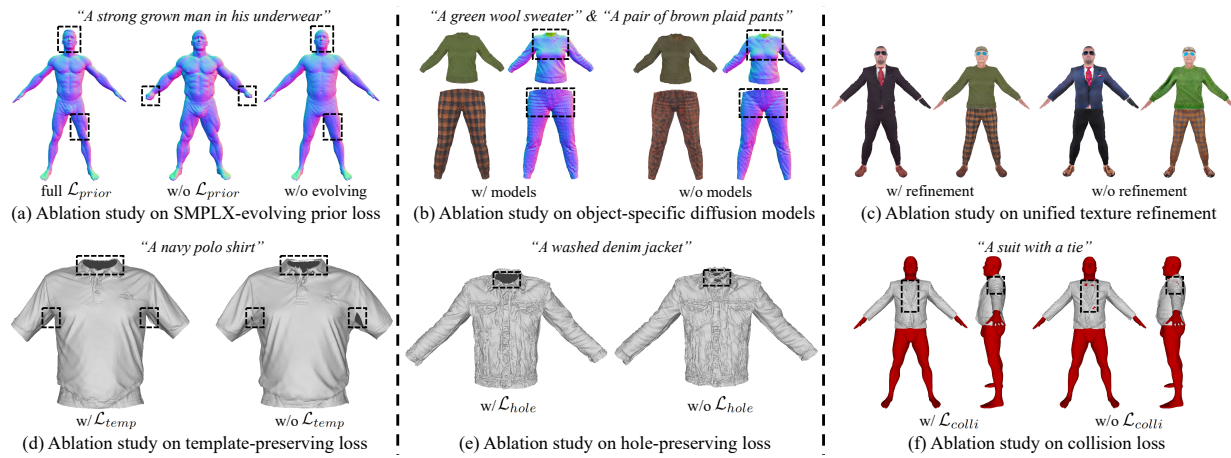


Fig. 8: Ablation Study of Barbie.

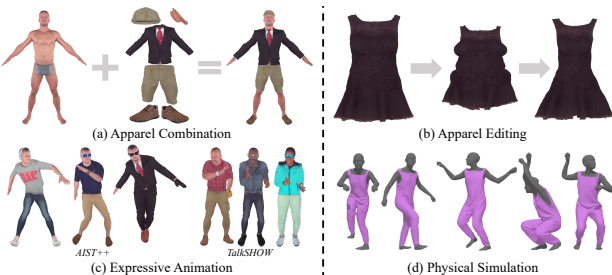


Fig. 9: Applications of Barbie.

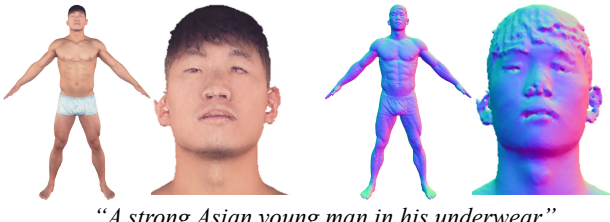


Fig. 10: Failure cases.

expressive G-Shell [63] representation, our method accurately captures non-watertight garment topology, supporting physical simulation [91] as shown in Fig. 9-(d).

V. LIMITATIONS AND FUTURE WORK

Limited by the resolution of G-Shell, our method struggles to accurately model highly complex geometries such as hair, ears, and other facial features, as shown in Fig. 10. Leveraging recent advances in 3D representations [97] provides a promising path toward improving the quality of generated digital humans. Furthermore, our reliance on SDS loss introduces significant computational overhead, restricting practical application. Especially for decoupled avatar generation, the training time increases linearly according to the number of components. Future work will focus on integrating diverse human datasets and advanced priors to enable efficient, high-quality 3D Barbie-style avatar generation, comparable to feed-forward methods [94].

VI. CONCLUSION

We propose Barbie, a novel text-guided framework for creating an animatable 3D avatar dressed in decoupled shoes and accessories, along with simulation-ready garments, resembling iconic Barbie dolls. Specifically, we employ an expressive G-Shell to uniformly represent both watertight and non-watertight meshes. Additionally, we introduce an efficient mSDF initialization and a hole-preserving loss to ensure well-defined open surface modeling. To guarantee the domain-specific fidelity of the generated human body and outfits, we suitably combine different specific expert T2I models for domain-specific knowledge. To mitigate the negative impacts caused by the over-strong generative priors of the expert models, we propose a series of solid regularization losses and optimization strategies to ensure geometric rationality and texture harmony of the generated results. Extensive experiments demonstrate that our approach not only outperforms compared methods in both dressed avatar and apparel generation tasks, but also facilitates seamless composition and editing of outfits, as well as expressive animation and physical simulation.

REFERENCES

- [1] OpenAI, “Chatgpt,” <https://openai.com/>, 2025.
- [2] A. Radford, J. W. Kim, C. Hallacy, A. Ramesh, G. Goh, S. Agarwal, G. Sastry, A. Askell, P. Mishkin, J. Clark *et al.*, “Learning transferable visual models from natural language supervision,” in *Proc. Int. Conf. Mach. Learn.*, 2021, pp. 8748–8763.
- [3] N. Mohammad Khalid, T. Xie, E. Beilovsky, and T. Popa, “Clipmesh: Generating textured meshes from text using pretrained image-text models,” in *ACM SIGGRAPH Asia*, 2022, pp. 1–8.
- [4] Y. Lu, X. Yang, X. Li, X. E. Wang, and W. Y. Wang, “Llmscore: Unveiling the power of large language models in text-to-image synthesis evaluation,” in *Adv. Neural Inf. Process. Syst.*, vol. 36, 2023, pp. 23 075–23 093.
- [5] K. Huang, K. Sun, E. Xie, Z. Li, and X. Liu, “T2i-compbench: A comprehensive benchmark for open-world compositional text-to-image generation,” in *Adv. Neural Inf. Process. Syst.*, vol. 36, 2023, pp. 78 723–78 747.
- [6] X. Zhang, J. Zhang, C. Zhang, J. H. Liew, H. Zhang, Y. Yang, and J. Feng, “Avatarstudio: High-fidelity and animatable 3d avatar creation from text,” *Int. J. Comput. Vis.*, pp. 1–19, 2025.
- [7] A. Jain, B. Mildenhall, J. T. Barron, P. Abbeel, and B. Poole, “Zero-shot text-guided object generation with dream fields,” in *Proc. IEEE Conf. Comput. Vis. Pattern Recogn.*, 2022, pp. 867–876.

[8] A. Sanghi, H. Chu, J. G. Lambourne, Y. Wang, C.-Y. Cheng, M. Fumero, and K. R. Malekshan, “Clip-forge: Towards zero-shot text-to-shape generation,” in *Proc. IEEE Conf. Comput. Vis. Pattern Recogn.*, 2022, pp. 18 603–18 613.

[9] R. Rombach, A. Blattmann, D. Lorenz, P. Esser, and B. Ommer, “High-resolution image synthesis with latent diffusion models,” in *Proc. IEEE Conf. Comput. Vis. Pattern Recogn.*, 2022, pp. 10 684–10 695.

[10] A. Ramesh, P. Dhariwal, A. Nichol, C. Chu, and M. Chen, “Hierarchical text-conditional image generation with clip latents,” *arXiv preprint arXiv:2204.06125*, 2022.

[11] C. Saharia, W. Chan, S. Saxena, L. Li, J. Whang, E. L. Denton, K. Ghasemipour, R. Gontijo Lopes, B. Karagol Ayan, T. Salimans *et al.*, “Photorealistic text-to-image diffusion models with deep language understanding,” in *Adv. Neural Inf. Process. Syst.*, vol. 35, 2022, pp. 36 479–36 494.

[12] B. Poole, A. Jain, J. T. Barron, and B. Mildenhall, “Dreamfusion: Text-to-3d using 2d diffusion,” in *Proc. Int. Conf. Learn. Represent.*, 2022.

[13] C.-H. Lin, J. Gao, L. Tang, T. Takikawa, X. Zeng, X. Huang, K. Kreis, S. Fidler, M.-Y. Liu, and T.-Y. Lin, “Magic3d: High-resolution text-to-3d content creation,” in *Proc. IEEE Conf. Comput. Vis. Pattern Recogn.*, 2023, pp. 300–309.

[14] R. Chen, Y. Chen, N. Jiao, and K. Jia, “Fantasia3d: Disentangling geometry and appearance for high-quality text-to-3d content creation,” in *Proc. IEEE Int. Conf. Comput. Vis.*, 2023, pp. 22 246–22 256.

[15] Z. Wang, C. Lu, Y. Wang, F. Bao, C. Li, H. Su, and J. Zhu, “Prolific-dreamer: High-fidelity and diverse text-to-3d generation with variational score distillation,” in *Adv. Neural Inf. Process. Syst.*, vol. 36, 2023, pp. 8406–8441.

[16] Y. Shi, P. Wang, J. Ye, L. Mai, K. Li, and X. Yang, “Mvdream: Multi-view diffusion for 3d generation,” in *Proc. Int. Conf. Learn. Represent.*, 2023.

[17] W. Li, R. Chen, X. Chen, and P. Tan, “Sweetdreamer: Aligning geometric priors in 2d diffusion for consistent text-to-3d,” in *Proc. Int. Conf. Learn. Represent.*, 2023.

[18] L. Qiu, G. Chen, X. Gu, Q. Zuo, M. Xu, Y. Wu, W. Yuan, Z. Dong, L. Bo, and X. Han, “Richdreamer: A generalizable normal-depth diffusion model for detail richness in text-to-3d,” in *Proc. IEEE Conf. Comput. Vis. Pattern Recogn.*, 2024, pp. 9914–9925.

[19] T. Yi, J. Fang, J. Wang, G. Wu, L. Xie, X. Zhang, W. Liu, Q. Tian, and X. Wang, “Gaussiandreamer: Fast generation from text to 3d gaussians by bridging 2d and 3d diffusion models,” in *Proc. IEEE Conf. Comput. Vis. Pattern Recogn.*, 2024, pp. 6796–6807.

[20] J. Tang, J. Ren, H. Zhou, Z. Liu, and G. Zeng, “Dreamgaussian: Generative gaussian splatting for efficient 3d content creation,” in *Proc. Int. Conf. Learn. Represent.*, 2023.

[21] Y. Liang, X. Yang, J. Lin, H. Li, X. Xu, and Y. Chen, “Luciddreamer: Towards high-fidelity text-to-3d generation via interval score matching,” in *Proc. IEEE Conf. Comput. Vis. Pattern Recogn.*, 2024, pp. 6517–6526.

[22] F. Hong, M. Zhang, L. Pan, Z. Cai, L. Yang, and Z. Liu, “Avatarclip: zero-shot text-driven generation and animation of 3d avatars,” *ACM Trans. Graph.*, vol. 41, no. 4, pp. 1–19, 2022.

[23] T. Liao, H. Yi, Y. Xiu, J. Tang, Y. Huang, J. Thies, and M. J. Black, “Tada! text to animatable digital avatars,” in *Proc. Int. Conf. 3D Vision*, 2024, pp. 1508–1519.

[24] N. Kolotouros, T. Alldieck, A. Zanfir, E. Bazavan, M. Fieraru, and C. Sminchisescu, “Dreamhuman: Animatable 3d avatars from text,” in *Adv. Neural Inf. Process. Syst.*, vol. 36, 2023, pp. 10 516–10 529.

[25] Y. Cao, Y.-P. Cao, K. Han, Y. Shan, and K.-Y. K. Wong, “Dreamavatar: Text-and-shape guided 3d human avatar generation via diffusion models,” in *Proc. IEEE Conf. Comput. Vis. Pattern Recogn.*, 2024, pp. 958–968.

[26] Y. Yuan, X. Li, Y. Huang, S. De Mello, K. Nagano, J. Kautz, and U. Iqbal, “Gavatar: Animatable 3d gaussian avatars with implicit mesh learning,” in *Proc. IEEE Conf. Comput. Vis. Pattern Recogn.*, 2024, pp. 896–905.

[27] Y. Xu, Z. Yang, and Y. Yang, “Seeavatar: Photorealistic text-to-3d avatar generation with constrained geometry and appearance,” *arXiv preprint arXiv:2312.08889*, 2023.

[28] S. Huang, Z. Yang, L. Li, Y. Yang, and J. Jia, “Avatarfusion: Zero-shot generation of clothing-decoupled 3d avatars using 2d diffusion,” in *Proc. ACM Int. Conf. Multimedia*, 2023, pp. 5734–5745.

[29] R. Jiang, C. Wang, J. Zhang, M. Chai, M. He, D. Chen, and J. Liao, “Avatarcraft: Transforming text into neural human avatars with parameterized shape and pose control,” in *Proc. IEEE Int. Conf. Comput. Vis.*, 2023, pp. 14 371–14 382.

[30] H. Zhang, B. Chen, H. Yang, L. Qu, X. Wang, L. Chen, C. Long, F. Zhu, D. Du, and M. Zheng, “Avatarverse: High-quality & stable 3d avatar creation from text and pose,” in *Proc. AAAI Conf. Artif. Intell.*, vol. 38, no. 7, 2024, pp. 7124–7132.

[31] Y. Huang, J. Wang, A. Zeng, H. Cao, X. Qi, Y. Shi, Z.-J. Zha, and L. Zhang, “Dreamwaltz: Make a scene with complex 3d animatable avatars,” in *Adv. Neural Inf. Process. Syst.*, vol. 36, 2023, pp. 4566–4584.

[32] X. Liu, X. Zhan, J. Tang, Y. Shan, G. Zeng, D. Lin, X. Liu, and Z. Liu, “Humangaussian: Text-driven 3d human generation with gaussian splatting,” in *Proc. IEEE Conf. Comput. Vis. Pattern Recogn.*, 2024, pp. 6646–6657.

[33] Y. Wang, J. Ma, R. Shao, Q. Feng, Y.-K. Lai, Y. Liu, and K. Li, “Humancoser: Layered 3d human generation via semantic-aware diffusion model,” in *Proc. IEEE Int. Symp. Mixed Augment. Real.*, 2024, pp. 436–445.

[34] X. Huang, R. Shao, Q. Zhang, H. Zhang, Y. Feng, Y. Liu, and Q. Wang, “Humannorm: Learning normal diffusion model for high-quality and realistic 3d human generation,” in *Proc. IEEE Conf. Comput. Vis. Pattern Recogn.*, 2024, pp. 4568–4577.

[35] J. Wang, Y. Liu, Z. Dou, Z. Yu, Y. Liang, X. Li, W. Wang, R. Xie, and L. Song, “Disentangled clothed avatar generation from text descriptions,” in *Proc. Eur. Conf. Comput. Vis.*, 2024, pp. 381–401.

[36] Y. Ma, Z. Lin, J. Ji, Y. Fan, X. Sun, and R. Ji, “X-oscar: A progressive framework for high-quality text-guided 3d animatable avatar generation,” in *Proc. Int. Conf. Mach. Learn.*, 2024, pp. 33 826–33 838.

[37] J. Dong, Q. Fang, Z. Huang, X. Xu, J. Wang, S. Peng, and B. Dai, “Tela: Text to layer-wise 3d clothed human generation,” in *Proc. Eur. Conf. Comput. Vis.*, 2024, pp. 19–36.

[38] J. Gong, S. Ji, L. G. Foo, K. Chen, H. Rahmani, and J. Liu, “Laga: Layered 3d avatar generation and customization via gaussian splatting,” *arXiv preprint arXiv:2405.12663*, 2024.

[39] B. Li, X. Li, Y. Jiang, T. Xie, F. Gao, H. Wang, Y. Yang, and C. Jiang, “Garmentdreamer: 3dgs guided garment synthesis with diverse geometry and texture details,” *arXiv preprint arXiv:2405.12420*, 2024.

[40] Y. Liu, J. Tang, C. Zheng, S. Zhang, J. Hao, J. Zhu, and D. Huang, “Clothedreamer: Text-guided garment generation with 3d gaussians,” *arXiv preprint arXiv:2406.16815*, 2024.

[41] M. Loper, N. Mahmood, J. Romero, G. Pons-Moll, and M. J. Black, “Smpl: a skinned multi-person linear model,” *ACM Trans. Graph.*, vol. 34, no. 6, pp. 1–16, 2015.

[42] G. Pavlakos, V. Choutas, N. Ghorbani, T. Bolkart, A. A. Osman, D. Tzionas, and M. J. Black, “Expressive body capture: 3d hands, face, and body from a single image,” in *Proc. IEEE Conf. Comput. Vis. Pattern Recogn.*, 2019, pp. 10 975–10 985.

[43] Q. Ma, J. Yang, A. Ranjan, S. Pujades, G. Pons-Moll, S. Tang, and M. J. Black, “Learning to dress 3d people in generative clothing,” in *Proc. IEEE Conf. Comput. Vis. Pattern Recogn.*, 2020, pp. 6469–6478.

[44] A. Ranjan, T. Bolkart, S. Sanyal, and M. J. Black, “Generating 3d faces using convolutional mesh autoencoders,” in *Proc. Eur. Conf. Comput. Vis.*, 2018, pp. 704–720.

[45] X. Chen, T. Jiang, J. Song, J. Yang, M. J. Black, A. Geiger, and O. Hilliges, “gdna: Towards generative detailed neural avatars,” in *Proc. IEEE Conf. Comput. Vis. Pattern Recogn.*, 2022, pp. 20 427–20 437.

[46] C. Schuhmann, R. Beaumont, R. Vencu, C. Gordon, R. Wightman, M. Cherti, T. Coombes, A. Katta, C. Mullis, M. Wortsman *et al.*, “Laion-5b: An open large-scale dataset for training next generation image-text models,” in *Adv. Neural Inf. Process. Syst.*, vol. 35, 2022, pp. 25 278–25 294.

[47] B. Mildenhall, P. P. Srinivasan, M. Tancik, J. T. Barron, R. Ramamoorthi, and R. Ng, “Nerf: Representing scenes as neural radiance fields for view synthesis,” in *Proc. Eur. Conf. Comput. Vis.*, 2020, pp. 405–421.

[48] P. Wang, L. Liu, Y. Liu, C. Theobalt, T. Komura, and W. Wang, “Neus: Learning neural implicit surfaces by volume rendering for multi-view reconstruction,” in *Adv. Neural Inf. Process. Syst.*, vol. 34, 2021, pp. 27 171–27 183.

[49] T. Müller, A. Evans, C. Schied, and A. Keller, “Instant neural graphics primitives with a multiresolution hash encoding,” *ACM Trans. Graph.*, vol. 41, no. 4, pp. 1–15, 2022.

[50] B. Kerbl, G. Kopanas, T. Leimkühler, and G. Drettakis, “3d gaussian splatting for real-time radiance field rendering,” *ACM Trans. Graph.*, vol. 42, no. 4, pp. 1–14, 2023.

[51] T. Shen, J. Gao, K. Yin, M.-Y. Liu, and S. Fidler, “Deep marching tetrahedra: a hybrid representation for high-resolution 3d shape synthesis,” in *Adv. Neural Inf. Process. Syst.*, vol. 34, 2021, pp. 6087–6101.

[52] S. Laine, J. Hellsten, T. Karras, Y. Seol, J. Lehtinen, and T. Aila, “Modular primitives for high-performance differentiable rendering,” *ACM Trans. Graph.*, vol. 39, no. 6, pp. 1–14, 2020.

[53] M. Cherti, R. Beaumont, R. Wightman, M. Wortsman, G. Ilharco, C. Gordon, C. Schuhmann, L. Schmidt, and J. Jitsev, “Reproducible scaling laws for contrastive language-image learning,” in *Proc. IEEE Conf. Comput. Vis. Pattern Recogn.*, 2023, pp. 2818–2829.

[54] P. J. Chia, G. Attanasio, F. Bianchi, S. Terragni, A. R. Magalhães, D. Goncalves, C. Greco, and J. Tagliabue, “Contrastive language and vision learning of general fashion concepts,” *Scientific Reports*, vol. 12, no. 1, p. 18958, 2022.

[55] X. Cheng, T. Yang, J. Wang, Y. Li, L. Zhang, J. Zhang, and L. Yuan, “Progressive3d: Progressively local editing for text-to-3d content creation with complex semantic prompts,” in *Proc. Int. Conf. Learn. Represent.*, 2023.

[56] A. Paszke, S. Gross, F. Massa, A. Lerer, J. Bradbury, G. Chanan, T. Killeen, Z. Lin, N. Gimelshein, L. Antiga *et al.*, “Pytorch: An imperative style, high-performance deep learning library,” in *Adv. Neural Inf. Process. Syst.*, vol. 32, 2019.

[57] Y.-C. Guo, Y.-T. Liu, R. Shao, C. Laforte, V. Voleti, G. Luo, C.-H. Chen, Z.-X. Zou, C. Wang, Y.-P. Cao, and S.-H. Zhang, “threestudio: A unified framework for 3d content generation,” <https://github.com/threestudio-project/threestudio>, 2023.

[58] D. Li, J. Li, H. Le, G. Wang, S. Savarese, and S. C. Hoi, “Lavis: A library for language-vision intelligence,” *arXiv preprint arXiv:2209.09019*, 2022.

[59] J. Li, D. Li, C. Xiong, and S. Hoi, “Blip: Bootstrapping language-image pre-training for unified vision-language understanding and generation,” in *Proc. Int. Conf. Mach. Learn.*, 2022, pp. 12 888–12 900.

[60] J. Li, D. Li, S. Savarese, and S. Hoi, “Blip-2: Bootstrapping language-image pre-training with frozen image encoders and large language models,” in *Proc. Int. Conf. Mach. Learn.*, 2023, pp. 19 730–19 742.

[61] T. Alldieck, H. Xu, and C. Sminchisescu, “imghum: Implicit generative models of 3d human shape and articulated pose,” in *Proc. IEEE Int. Conf. Comput. Vis.*, 2021, pp. 5461–5470.

[62] L. Zhang, A. Rao, and M. Agrawala, “Adding conditional control to text-to-image diffusion models,” in *Proc. IEEE Int. Conf. Comput. Vis.*, 2023, pp. 3836–3847.

[63] Z. Liu, Y. Feng, Y. Xiu, W. Liu, L. Paull, M. J. Black, and B. Schölkopf, “Ghost on the shell: An expressive representation of general 3d shapes,” in *Proc. Int. Conf. Learn. Represent.*, 2024.

[64] Y. Huang, J. Wang, A. Zeng, Z.-J. Zha, L. Zhang, and X. Liu, “Dreamwaltz-g: Expressive 3d gaussian avatars from skeleton-guided 2d diffusion,” *arXiv preprint arXiv:2409.17145*, 2024.

[65] H. Chen, B. Peng, Y. Tao, and J. Zhang, “D³-human: Dynamic disentangled digital human from monocular video,” *arXiv preprint arXiv:2501.01589*, 2025.

[66] Y.-T. Liu, X. Gao, W. Chen, J. Yang, X. Meng, B. Yang, and L. Gao, “Dreamudf: Generating unsigned distance fields from a single image,” *ACM Trans. Graph.*, vol. 43, no. 6, pp. 1–21, 2024.

[67] H. Chen, Y. Yao, and J. Zhang, “Neural-abc: neural parametric models for articulated body with clothes,” *IEEE Trans. Vis. Comput. Graph.*, vol. 31, no. 2, pp. 1478–1495, 2024.

[68] J. Chibane, G. Pons-Moll *et al.*, “Neural unsigned distance fields for implicit function learning,” in *Adv. Neural Inf. Process. Syst.*, vol. 33, 2020, pp. 21 638–21 652.

[69] X. Li, Y. Yuan, S. De Mello, G. Daviet, J. Leaf, M. Macklin, J. Kautz, and U. Iqbal, “Simavatar: Simulation-ready avatars with layered hair and clothing,” *arXiv preprint arXiv:2412.09545*, 2024.

[70] K. He, K. Yao, Q. Zhang, J. Yu, L. Liu, and L. Xu, “Dresscode: Autoregressively sewing and generating garments from text guidance,” *ACM Trans. Graph.*, vol. 43, no. 4, pp. 1–13, 2024.

[71] S. Saito, Z. Huang, R. Natsume, S. Morishima, A. Kanazawa, and H. Li, “Pifu: Pixel-aligned implicit function for high-resolution clothed human digitization,” in *Proc. IEEE Conf. Comput. Vis. Pattern Recogn.*, 2019, pp. 2304–2314.

[72] S. Saito, T. Simon, J. Saragih, and H. Joo, “Pifuhd: Multi-level pixel-aligned implicit function for high-resolution 3d human digitization,” in *Proc. IEEE Conf. Comput. Vis. Pattern Recogn.*, 2020, pp. 84–93.

[73] Z. Zheng, T. Yu, Y. Liu, and Q. Dai, “Pamir: Parametric model-conditioned implicit representation for image-based human reconstruction,” *IEEE Trans. Pattern Anal. Mach. Intell.*, vol. 44, no. 6, pp. 3170–3184, 2021.

[74] T. Alldieck, M. Magnor, B. L. Bhatnagar, C. Theobalt, and G. Pons-Moll, “Learning to reconstruct people in clothing from a single rgb camera,” in *Proc. IEEE Conf. Comput. Vis. Pattern Recogn.*, 2019, pp. 1175–1186.

[75] X. Li, J. Huang, J. Zhang, X. Sun, H. Xuan, Y.-K. Lai, Y. Xie, J. Yang, and K. Li, “Learning to infer inner-body under clothing from monocular video,” *IEEE Trans. Vis. Comput. Graph.*, vol. 29, no. 12, pp. 5083–5096, 2022.

[76] B. Jiang, Y. Hong, H. Bao, and J. Zhang, “Selfrecon: Self reconstruction your digital avatar from monocular video,” in *Proc. IEEE Conf. Comput. Vis. Pattern Recogn.*, 2022, pp. 5605–5615.

[77] S. Pujades, B. Mohler, A. Thaler, J. Tesch, N. Mahmood, N. Hesse, H. H. Bülthoff, and M. J. Black, “The virtual caliper: rapid creation of metrically accurate avatars from 3d measurements,” *IEEE Trans. Vis. Comput. Graph.*, vol. 25, no. 5, pp. 1887–1897, 2019.

[78] A. Genay, A. Lécuyer, and M. Hachet, “Being an avatar “for real”: a survey on virtual embodiment in augmented reality,” *IEEE Trans. Vis. Comput. Graph.*, vol. 28, no. 12, pp. 5071–5090, 2021.

[79] F. Weidner, G. Boettcher, S. A. Arboleda, C. Diao, L. Sinani, C. Kunert, C. Gerhardt, W. Broll, and A. Raake, “A systematic review on the visualization of avatars and agents in ar & vr displayed using head-mounted displays,” *IEEE Trans. Vis. Comput. Graph.*, vol. 29, no. 5, pp. 2596–2606, 2023.

[80] Z. Chai, C. Tang, Y. Wong, and M. Kankanhalli, “Star: skeleton-aware text-based 4d avatar generation with in-network motion retargeting,” *arXiv preprint arXiv:2406.04629*, 2024.

[81] B. Jiang, J. Zhang, Y. Hong, J. Luo, L. Liu, and H. Bao, “Bcnet: Learning body and cloth shape from a single image,” in *Proc. Eur. Conf. Comput. Vis.*, 2020, pp. 18–35.

[82] B. L. Bhatnagar, G. Tiwari, C. Theobalt, and G. Pons-Moll, “Multi-garment net: Learning to dress 3d people from images,” in *Proc. IEEE Int. Conf. Comput. Vis.*, 2019, pp. 5420–5430.

[83] T. Kim, B. Kim, S. Saito, and H. Joo, “Gala: Generating animatable layered assets from a single scan,” in *Proc. IEEE Conf. Comput. Vis. Pattern Recogn.*, 2024, pp. 1535–1545.

[84] S. Lin, Z. Li, Z. Su, Z. Zheng, H. Zhang, and Y. Liu, “Layga: Layered gaussian avatars for animatable clothing transfer,” in *ACM SIGGRAPH*, 2024, pp. 1–11.

[85] J. J. Park, P. Florence, J. Straub, R. Newcombe, and S. Lovegrove, “Deepsdf: Learning continuous signed distance functions for shape representation,” in *Proc. IEEE Conf. Comput. Vis. Pattern Recogn.*, 2019, pp. 165–174.

[86] Y. Feng, J. Yang, M. Pollefeys, M. J. Black, and T. Bolkart, “Capturing and animation of body and clothing from monocular video,” in *ACM SIGGRAPH Asia*, 2022, pp. 1–9.

[87] H. Zhang, Y. Feng, P. Kulits, Y. Wen, J. Thies, and M. J. Black, “Teca: Text-guided generation and editing of compositional 3d avatars,” in *Proc. Int. Conf. 3D Vision*, 2024, pp. 1520–1530.

[88] Y. Feng, W. Liu, T. Bolkart, J. Yang, M. Pollefeys, and M. J. Black, “Learning disentangled avatars with hybrid 3d representations,” *arXiv preprint arXiv:2309.06441*, 2023.

[89] E. Corona, A. Pumarola, G. Alenya, G. Pons-Moll, and F. Moreno-Noguer, “Smplicit: Topology-aware generative model for clothed people,” in *Proc. IEEE Conf. Comput. Vis. Pattern Recogn.*, 2021, pp. 11 875–11 885.

[90] K. Simonyan and A. Zisserman, “Very deep convolutional networks for large-scale image recognition,” in *Proc. Int. Conf. Learn. Represent.*, 2014.

[91] A. Grigorev, G. Becherini, M. Black, O. Hilliges, and B. Thomaszewski, “Contourcraft: Learning to resolve intersections in neural multi-garment simulations,” in *ACM SIGGRAPH*, 2024, pp. 1–10.

[92] H. Yi, H. Liang, Y. Liu, Q. Cao, Y. Wen, T. Bolkart, D. Tao, and M. J. Black, “Generating holistic 3d human motion from speech,” in *Proc. IEEE Conf. Comput. Vis. Pattern Recogn.*, 2023, pp. 469–480.

[93] R. Li, S. Yang, D. A. Ross, and A. Kanazawa, “Learn to dance with aist++: Music conditioned 3d dance generation,” *arXiv preprint arXiv:2101.08779*, 2021.

[94] Y. He, Y. Zhou, W. Zhao, Z. Wu, K. Xiao, W. Yang, Y.-J. Liu, and X. Han, “Stdgen: Semantic-decomposed 3d character generation from single images,” *arXiv preprint arXiv:2411.05738*, 2024.

[95] J. Xiang, Z. Lv, S. Xu, Y. Deng, R. Wang, B. Zhang, D. Chen, X. Tong, and J. Yang, “Structured 3d latents for scalable and versatile 3d generation,” *arXiv preprint arXiv:2412.01506*, 2024.

[96] Y. Huang, H. Yi, Y. Xiu, T. Liao, J. Tang, D. Cai, and J. Thies, “Tech: Text-guided reconstruction of lifelike clothed humans,” in *Proc. Int. Conf. 3D Vision*, 2024, pp. 1531–1542.

[97] B. Zhang, J. Tang, M. Niessner, and P. Wonka, “3dshape2vecset: A 3d shape representation for neural fields and generative diffusion models,” *ACM Trans. Graph.*, vol. 42, no. 4, pp. 1–16, 2023.

[98] B. Zhang, J. Ren, and P. Wonka, “Geometry distributions,” *arXiv preprint arXiv:2412.01506*, 2024.

[99] S. Wu, Y. Yan, Y. Li, Y. Cheng, W. Zhu, K. Gao, X. Li, and G. Zhai, “Ganhead: Towards generative animatable neural head avatars,” in *Proceedings of the IEEE/CVF conference on computer vision and pattern recognition*, 2023, pp. 437–447.



Xiaokun Sun is currently a Ph.D. candidate at the School of Intelligence Science and Technology, Nanjing University (Suzhou campus). Before this, he received his Master's degree from Tianjin University in 2024. His research interests focus on human-centric 3D digitization.



Zhenyu Zhang is currently an associate professor at the School of Intelligent Science and Technology, Nanjing University (Suzhou campus). He got his Ph.D degree from Nanjing University of Science and Technology in 2020. During 2020-2023, he worked as a staff research scientist at Tencent YouTu Lab. His research interests include 3D modeling, rendering, and generation. His long-term research objective is to create an interactive world simulator from real-world knowledge and human prior.



Ying Tai is currently an associate professor at the School of Intelligence Science and Technology, Nanjing University (Suzhou Campus). He got his Ph.D. degree from Nanjing University of Science and Technology in 2017. During 2017-2023, he worked as a principal researcher and team lead at Tencent YouTu Lab. His research interests include Frontier Generative AI research and applications based on large vision and language models.



Hao Tang is a tenure-track Assistant Professor at Peking University, China. He earned a master's degree from Peking University, China, and a Ph.D. from the University of Trento, Italy. His research interests include AIGC, LLM, machine learning, computer vision, embodied AI, and their applications to scientific domains.



Zili Yi is currently an associate professor at the School of Intelligence Science and Technology, Nanjing University (Suzhou Campus). He got his Ph.D. degree from Memorial University of Newfoundland, Canada, in 2018. His main research interests include high-quality visual content generation, image/video editing, and multimodal controllable generation.



Jian Yang got his Ph.D. degree from Nanjing University of Science and Technology in 2002. He has authored more than 300 scientific papers in pattern recognition and computer vision. His papers have been cited more than 55000 times in Scholar Google. His research interests include pattern recognition, computer vision, and machine learning.